Applied Catalysis A: General 525 (2016) 76–84

Contents lists available at ScienceDirect

Applied Catalysis A: General

journal homepage: www.elsevier.com/locate/apcata

Insight into CH_x formation in Fischer–Tropsch synthesis on the hexahedron Co catalyst: Effect of surface structure on the preferential mechanism and existence form

Riguang Zhang [a], Fu Liu [a], Qiang Wang [b], Baojun Wang [a,*], Debao Li [b]

[a] Key Laboratory of Coal Science and Technology of Ministry of Education and Shanxi Province, Taiyuan University of Technology, Taiyuan 030024, Shanxi, PR China

[b] State Key Laboratory of Coal Conversion, Institute of Coal Chemistry, Chinese Academy of Science, Taiyuan 030001, Shanxi, PR China

ARTICLE INFO

Article history:
Received 17 May 2016
Received in revised form 10 July 2016
Accepted 11 July 2016
Available online 14 July 2016

Keywords:
Syngas
CH_x formation
Cobalt
Methanol
Density functional theory

ABSTRACT

Spin-polarized density functional theory calculations have been performed to investigate the preferential mechanism of CH_x(x = 1–3) formation in Fischer-Tropsch synthesis on only the hexahedron Co($10\bar{1}0$)-A and Co($10\ \bar{1}0$) surfaces. Our results show that CO hydrogenation to CHO is favored compared to CO direct dissociation and hydrogenation to COH on these two surfaces. Starting from C and CHO, we further seek out the optimal pathways of CH_x formation, suggesting that CH_x is mainly formed through H-assisted CO dissociation pathways on Co($10\bar{1}0$)-A surface, in which CH is form via CHO dissociation, CH_2 and CH_3 are formed through CH_2O with the direct and H-assisted dissociation, respectively; meanwhile, CH_2 hydrogenation also contributes to CH_3 formation; CH_2 and CH_3 are the surface abundant species on Co($10\bar{1}0$)-A surface. However, on Co($10\bar{1}1$) surface, CH_x species is formed through CO direct dissociation into C, followed by C successive hydrogenation, C and CH are the surface abundant species. Therefore, Co surface structure can affect the preferential formation pathways and the dominant existence form of CH_x species. Moreover, CH_3OH formation cannot compete with CH_x formation on Co($10\bar{1}0$)-A and Co($10\bar{1}1$) surfaces, considering both surfaces covering 63% of the total surface area exposed of hexahedron Co surfaces, which depends on the reaction conditions, particle size, catalyst support, carbon deposition and many other factors, the contribution to the overall CH_x sources from Co($10\bar{1}0$)-A and Co($10\bar{1}1$) surfaces even surpasses that of other hexahedron Co surfaces under the certain realistic conditions. As a result, the hexahedron Co surfaces exhibit high catalytic selectivity for CH_x formation, and provide more CH_x sources to participate into the F-T synthesis.

1. Introduction

The Fischer-Tropsch synthesis (FTS) is a set of chemical reactions that converts syngas ($CO + H_2$) into the long-chain alkanes, alkenes, and small amounts of oxygenates [1–3], Cobalt (Co) catalyst is widely used due to its high activity and selectivity towards the desired hydrocarbons, low intrinsic activity for water-gas-shift reaction and the relatively low cost [4–7]. To date, two accepted mechanisms have been proposed for syngas conversion to hydrocarbons, one is the carbide mechanism proposed by Fischer and Tropsch [8] with the C_1 intermediates formed by the direct C—O bond cleavage of CO into C, followed by the successive hydrogenation to CH_x intermediate; the other is CO insertion mechanism proposed by Pichler and Schulz [9] with the chain growth via CO insertion into CH_x to CH_xCO, followed by the C—O bond scission and further hydrogenation to hydrocarbons. Above two mechanism show that CH_x formation is one of the key steps involving in FTS process, thus, a fundamental understanding about the preferential mechanism of CH_x formation from syngas on Co-based catalysts is desired at a molecular level.

For CH_x(x = 1–3) formation, CO direct dissociation mechanism (the C—O bond scission followed by hydrogenation) or H-assisted CO dissociation mechanism via C_1 oxygenates has arouse certain concerns. Experimental [10–12] and theoretical [13–18] studies have suggested that the corrugated and stepped surfaces exhibit the enhanced activity of CO direct dissociation compared to the flat surface. For example, UHV studies have presented the undissociated CO absorbed on the flat Co(0001) surface under low pressure and 100–450 K [19]. Inderwildi et al. [20] have found that CH and CH_2 species come from CHO and CH_2O direct dissociation on

* Corresponding author at: No. 79 Yingze West Street, Taiyuan, 030024, PR China.
E-mail addresses: wangbaojun@tyut.edu.cn, quantumtyut@126.com (B. Wang).

http://dx.doi.org/10.1016/j.apcata.2016.07.007
0926-860X/

Co(0001) surface rather than CO direct dissociation. The studies by Ojeda et al. [21] on the flat Co(0001) surface have also shown that CO prefers to be hydrogenated to CHO, the further hydrogenation species CHOH and CH_2O are responsible for CH and CH_2 formations, respectively. Thus, H-assisted CO dissociation mechanism via C_1 oxygenates is suggested as an important mechanism for CH and CH_2 formations on the flat Co(0001) surface. However, on the corrugated and stepped Co surface, CO direct dissociation would be favorable. Ge et al. [15] have proposed that the corrugated Co(11$\bar{2}$4) and stepped Co(10$\bar{1}$2) surfaces can significantly enhance the reactivity by effectively reducing the activation barrier of CO direct dissociation compared to the flat Co(0001) surface [22,13]. Shetty et al. [18] have also clearly declared that CO direct dissociation is much more favorable than H-assisted CO dissociation for CH formation on Co(10$\bar{1}$0)-B surface. The studies by Liu et al. [17] supported that CO prefers to be the direct dissociation rather than being hydrogenated to CHO, followed by the C—O bond dissociation into CH on the corrugated Co(11$\bar{2}$1) and stepped Co(10$\bar{1}$1) surfaces, meanwhile, Liu et al. [16] also presented that besides CO direct dissociation, H-assisted CO dissociation is also responsible for CH_x formation on the corrugated Co(11$\bar{2}$0) and stepped Co(10$\bar{1}$2) surfaces. Huo et al. [23] and Helden et al. [24] further found that CH formation with H-assisted CO dissociation mechanism via CHO intermediate is more favorable than CO direct dissociation and C hydrogenation to CH on the double stepped Co(0001) and stepped Co(211) surfaces, respectively, and CH_2O dissociation via the C—O bond cleavage is responsible for CH_2 formation [23]. Recently, our studies [25] have investigated the C_2 hydrocarbons formation from syngas on fcc-Co(111) and the stepped Co(111) surfaces, respectively, the results indicate that CH is the dominant monomer formed by H-assisted CO dissociation, namely, $CO + H \rightarrow CHO \rightarrow CH + O$.

Above results for CH_x(x = 1–3) formation show that CO direct dissociation mechanism and/or H-assisted CO dissociation mechanism via C_1 oxygenates can be responsible for CH_x formation on different Co surfaces, which greatly depends on Co surface structure, namely, CH_x formation on Co surface is sensitive to surface structure.

On the other hand, for metal Co, it is well-known that Co can exist in two crystallographic structures, namely, the hexagonal close packed (hcp) phase and the face-centered cubic (fcc) phase, and both phases are observed in FTS [17]. The existence form of phase will depend on the conditions, particle size, catalyst support and promoter, carbon deposition and many other factors. The hcp structure is preferred for the bulk Co, when the crystallites with the Co particles is below 100 nm, the fcc phase are more stable the hcp phase [26,27]. On the other hand, when the temperature is above 695 K [28,29], the phase transition from hexahedron Co to face-centered cubic Co occurs, suggesting that the hcp Co exists in FTS process due to its low temperature of about 530 K [30,31], moreover, the hcp Co has higher FTS activity than fcc Co. Further, since our previous studies [25] have investigated the CH_x formation from syngas on fcc-Co(111) and the stepped Co(111) surfaces, as a result, in this study, we only focus on the hcp Co. It is worth noting that the morphology of the bulk hcp Co is a dihedral-like shape with two close-packed (0001) surfaces. Although (0001) surface has the very low surface energy, it covers only 18% of the total surface area exposed, the open Co(10$\bar{1}$1) and Co(10$\bar{1}$0)-A surfaces with the higher surface energy dominate 35% and 28% of the total surface area exposed, respectively [17]. In addition, for Co(10$\bar{1}$0) surface, the spacing between adjacent layers is alternately short or long, which are denoted as Co(10$\bar{1}$0)-A and Co(10$\bar{1}$0)-B surfaces, respectively, however, the full dynamic analyses demonstrated that the equilibrium surface structure is exclusively terminated with the short interlayer spacing outermost Co(10$\bar{1}$0)-A, which is unreconstructed [32–34]. Moreover, it is interesting to note that, although the active sites (such as step edges) on some reported hexahedron Co surfaces has the higher catalytic activity, typically they are unstable in nature, and their corresponding exposed surface area is very low [17]. Whereas, both Co(10$\bar{1}$1) and Co(10$\bar{1}$0)-A surfaces covering 35% and 28% of the total surface area exposed comes from its higher surface atomic density, relative lower surface energy.

So far, on the hexahedron Co(10$\bar{1}$1) and Co(10$\bar{1}$0)-A surfaces, there is few unequivocal results about the detailed preferential mechanism of CH_x(x = 1–3) formation and the dominant surface CH_x monomer, as well as the effect of the hexahedron Co surface structure on the preferential mechanism of CH_x formation, which are still open to discussion.

Thus, in this study, the detailed formation mechanism of CH_x monomer from syngas in FTS process on Co catalysts will be carried out on the hexahedron Co(10$\bar{1}$1) and Co(10$\bar{1}$0)-A surfaces using density functional theory (DFT) calculations together with the periodic slab models. The results of this work are expected to provide an instructive understanding at a molecular level about the preferential mechanism of CH_x formation, and the most favorable CH_x monomer, as well as the effect of the hexahedron Co surface structure on CH_x formation in FTS process.

2. Computational details

2.1. Computational methods

All calculations have been carried out using the periodic spin-polarized DFT implemented in the Vienna Ab Initio Simulation Package (VASP) [35,36]. The generalized gradient approximation with Perdew-Burke-Ernzerhof exchange-correlation functional (GGA-PBE) is used [37]. The kinetic energy cutoff for a plane wave basis set is 400 eV, a Monkhorst-Pack mesh k-points of $5 \times 5 \times 1$ is used [38], and the projector augmented wave pseudopotentials are used to describe the inner-shell electrons. When the change of total energy are converged to 5×10^{-6} eV/atom, and the forces on the ions are below 10^{-2} eV/Å, the optimization is thought to be converged. On the other hand, reaction pathways have been investigated using the climbing-image (CI-NEB) method [39,40]. Transition states have been optimized using the dimer method [41,42]. The structure of the transition state is deemed converged when the forces acting on the atoms are all less than 0.05 eV/Å and the structures are at a saddle point.

2.2. Surface model

A $p(3 \times 2)$ supercell for Co(10$\bar{1}$0)-A and Co(10$\bar{1}$1) surfaces with a 15 and 12 Å vacuum space has been employed, respectively. During the calculations, the uppermost two metal layers together with the adsorbed species are fully relaxed, the bottom layer is fixed at the Co bulk positions. For Co(10$\bar{1}$0)-A surface, four adsorption sites exist: Top, Bridge, Hcp and 4-fold hollow sites, as shown in Fig. 1(a). For Co(10$\bar{1}$1) surface, five adsorption sites exist: Top, Bridge, Hcp, Fcc and 4-fold hollow sites, as shown in Fig. 1(b).

For a reaction such as R (reactant) → P (product) on catalyst surface, the activation barrier (E_a) and reaction energy (ΔE) are calculated according to the following formulas:

$$E_a = E_{TS} - E_R$$

$$\Delta E = E_P - E_R$$

Where E_R and E_P are the total energies of the adsorbed reactant and product, respectively, and E_{TS} is the total energies of the transition state.

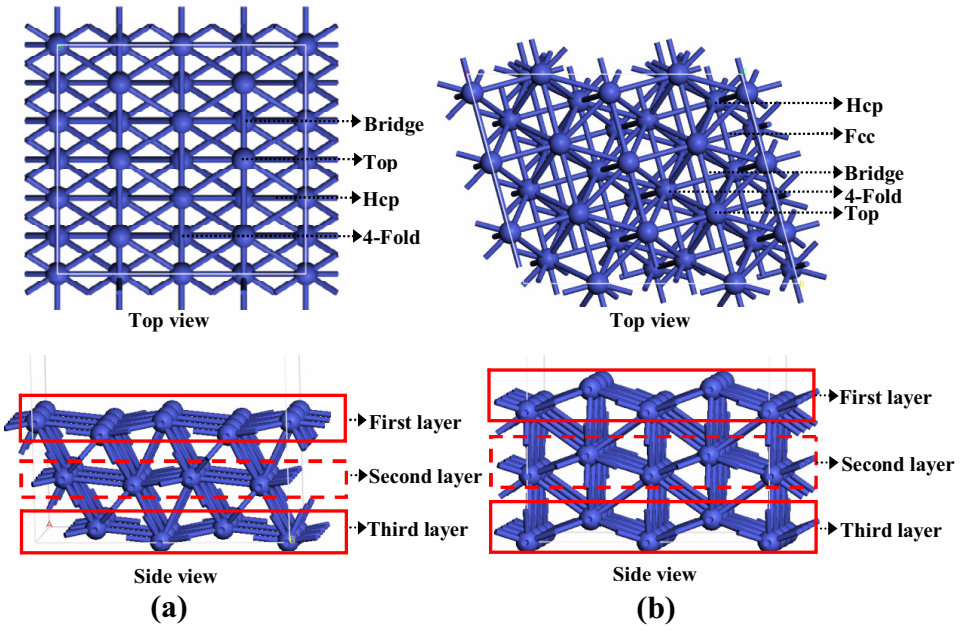

Fig. 1. The surface morphology and the corresponding adsorption sites of (a) Co(10$\bar{1}$0)-A and (b) Co(10$\bar{1}$1) surfaces.

3. Results and discussion

In order to investigate the formation mechanism of CH_x species, we firstly examine the adsorption of all possible species involved in CH_x formation from syngas on Co(10$\bar{1}$1) and Co(10$\bar{1}$0)-A surfaces, respectively. Here, only the most stable adsorption configurations are given in Figs. S1 and S2, the corresponding adsorption energies and key structural parameters are listed in Tables S1 and S2.

The adsorption energy (E_{ads}) is defined as follows:

$$E_{ads} = E_{(adsorbate/slab)} - E_{(slab)} - E_{(adsorbate)}$$

Where $E_{(adsorbate/slab)}$, $E_{(slab)}$ and $E_{(adsorbate)}$ are the total energies of the slab with the adsorbate in the equilibrium state, the slab surface and the free adsorbate, respectively. With this definition, more negative value of the adsorption energy reflect the strong interaction between the adsorbed species and the slab Co surface. Therefore, the stronger interaction would be more exothermic with more negative adsorption energies.

3.1. CO initial activation

For CO initial activation, as listed in Table 1, CO direct dissociation, CO hydrogenation to CHO or COH (R1-1–R1-3) have been considered on Co(10$\bar{1}$1) and Co(10$\bar{1}$0)-A surfaces, respectively. The corresponding potential energy profile together with the structures of initial states (ISs), transition states (TSs) and final states (FSs) are presented in Fig. 2.

On Co(10$\bar{1}$0)-A surface, CO direct dissociation (**R1-1**) goes through a transition state TS1-1 to form C + O, CO is adsorbed at the hcp site with the C—O bond length of 1.20 Å, in TS1-1, C migrates to the 4-fold hollow site, O tends to absorb at the neighboring hcp site, the corresponding C—O distance is extended to 1.88 Å, in the final state, the C—O distance is lengthened to 3.96 Å with the C and O atoms adsorbed at the 4-fold hollow site and hcp site, respectively, this elementary reaction is endothermic by 62.0 kJ mol^{-1}, and it has an activation barrier of 188.9 kJ mol^{-1}. For CO hydrogenation to CHO in **R1-2**, in its initial state, CO and H are adsorbed at two adjacent hcp sites, respectively, the C—H distance is shortened to 1.13 Å in TS1-2 from 2.63 Å in CO + H(1), this elementary reaction needs to overcome an activation barrier of 113.6 kJ mol^{-1}, which is endothermic by 92.1 kJ mol^{-1}. For CO hydrogenation to COH in **R1-3**, the O—H distance decreases to 1.29 Å in TS1-3 from 3.55 Å in CO + H(2), this elementary reaction has an activation barrier of 165.9 kJ mol^{-1} with the reaction energy of 84.8 kJ mol^{-1}

On Co(10$\bar{1}$1) surface, in **R1-1′**, starting from CO adsorbed at the hcp site, CO direct dissociation can form C and O via a transition state TS1-1′; in TS1-1′, C stays at the 4-fold hollow site, O tends to absorb at the adjacent 4-fold hollow site, the C—O distance is extended to 1.86 Å from 1.22 Å in CO, in the final state, the C—O distance is increased to 2.88 Å with C and O adsorbed at two adjacent 4-fold hollow sites, respectively, this elementary reaction is exothermic by 40.1 kJ mol^{-1}, and it has an activation barrier of 143.7 kJ mol^{-1}. In **R1-2′**, CHO formation starts with CO and H adsorbed at the 4-fold hollow and hcp sites, respectively, the C—H distance is shortened to 1.39 Å in TS1-2′ from 2.85 Å in CO + H, this elementary reaction needs to overcome an activation barrier of 102.8 kJ mol^{-1}, and it is endothermic by 66.5 kJ mol^{-1}. In **R1-3′**, CO hydrogenation can form COH via TS1-3′, the O—H distance decreases to 1.35 Å in TS1-3′ from 2.85 Å in CO + H, this elementary reaction has an activation barrier of 151.0 kJ·mol^{-1} with the reaction energy of 61.3 kJ mol^{-1}.

On the basis of above results, we can obtain that when CO and H are co-adsorbed on Co(10$\bar{1}$0)-A and Co(10$\bar{1}$1) surfaces, respectively, CO hydrogenation to CHO is more favorable than other two reactions in kinetics. The differences of activation barriers between Co(10$\bar{1}$0)-A and Co(10$\bar{1}$1) surfaces are 45.2, 10.8 and 14.9 kJ mol^{-1} for CO direct dissociation, CHO and COH formations, respectively, suggesting that CO direct dissociation is the most structurally sensitive reactions on Co catalysts.

3.2. CH_x(x = 1–3) formation

For CH_x formation from syngas, two accepted mechanisms exist, one is the direct C—O bond cleavage of CO to produce C, followed by C successive hydrogenation to CH_x species, the other is CO hydrogenation to CH_xO or CH_xOH intermediates, followed by its direct or H-assisted C—O bond cleavage to CH_x species. In this study, above two mechanisms have been examined. Starting from CO activation, the activation barriers and reaction energies of all possible reactions involving in CH_x formation from syngas on Co(10$\bar{1}$0)-A and

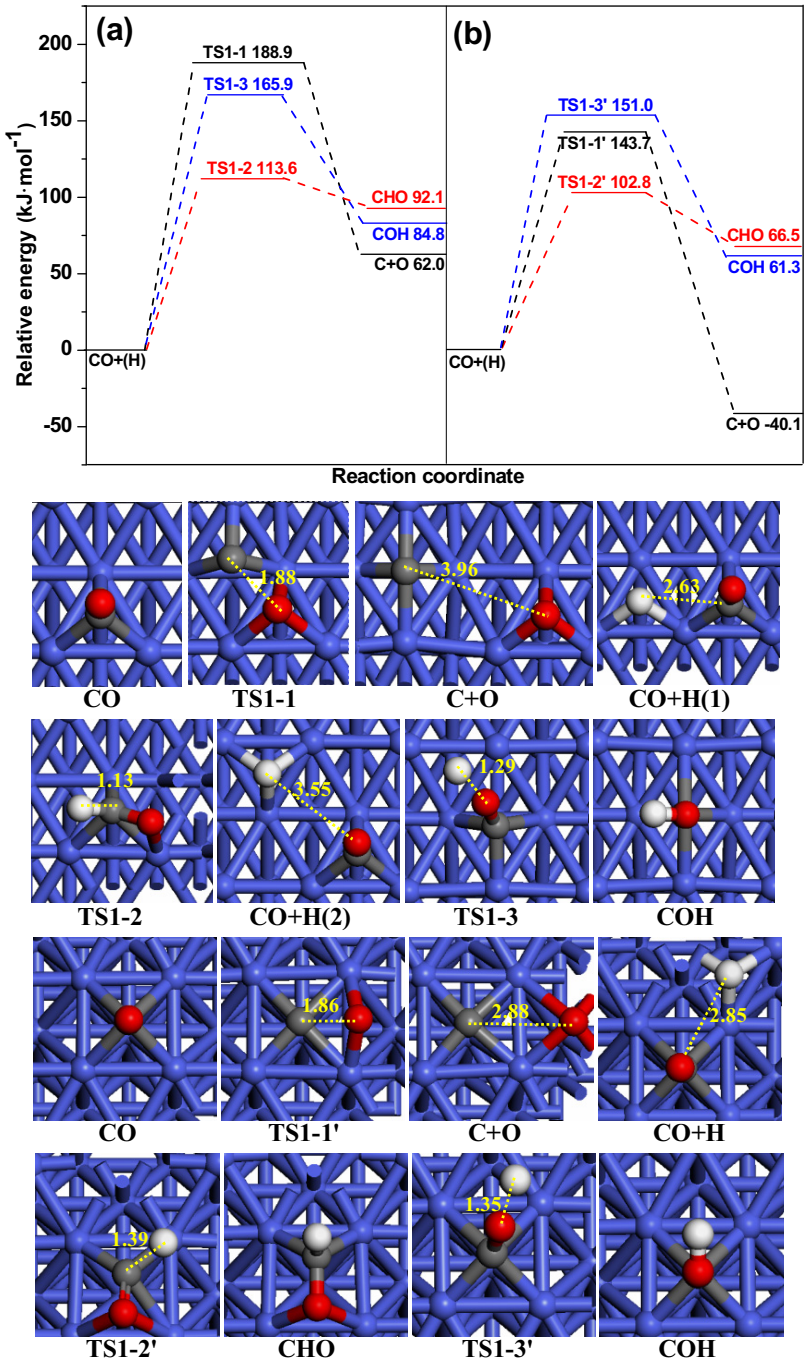

Fig. 2. The potential energy profile of CO activation together with the structures of initial states (ISs), transition states (TSs) and final states (FSs) on Co(10$\bar{1}$0)-A and (b) Co(10$\bar{1}$1) surfaces. The Co, C, H and O atoms are shown in the purple, grey, white and red balls, respectively. Bond lengths are in Å (for interpretation of the references to colour in this figure legend, the reader is referred to the web version of this article).

Co(10$\bar{1}$1) surfaces have been listed in Table 1. Figs. S3–S8 in the Supplementary material present the potential energy profiles of all possible pathways of CH_x formation together with ISs, TSs and FSs. Fig. 3 only displays the potential energy profiles of the most favorable H-assisted CO dissociation pathway and the hydrogenation pathway for CH_x formation on Co(10$\bar{1}$0)-A and Co(10$\bar{1}$1) surfaces, respectively.

3.2.1. CH formation

Starting from C + H, CHO, CHO + H and CHOH species, five pathways with six reactions (R2–1kR2-6) for CH formation have been considered, as shown in Table 1.

As depicted in Fig. 3(a), on Co(10$\bar{1}$0)-A surface, with respect to CO + H species, the CO direct dissociation pathway of CO + H → C + O + H → CH + O (R1-1, R2-1) has the overall barrier and reaction energy of 188.9 and 27.2 kJ mol^{-1}, respectively. However, the optimal H-assisted CO dissociation pathway of CO + H → CHO → CH + O (R1-2, R2-3) has the overall barrier and reaction energy of 143.3 and 11.8 kJ mol^{-1}, respectively, which are also lower than that for CO hydrogenation to COH (165.9 and 84.8 kJ mol^{-1}), suggesting that H-assisted CO dissociation pathway is dominantly responsible for CH formation on Co(10$\bar{1}$0)-A surface.

On Co(10$\bar{1}$1) surface, as shown in Fig. 3(b), with respect to CO + H species, CO direct dissociation pathway,

Table 1
All possible elementary reactions and the corresponding activation barriers (E_a/kJ mol^{-1}) and reaction energies (ΔE/kJ mol^{-1}) involving in CH_x formation from syngas on Co() and Co()-A surfaces.

Reactions		Co(10$\bar{1}$0)-A surface		Co(10$\bar{1}$1) surface	
		*E*a	ΔE	*E*a	ΔE
R1-1	CO → C + O	188.9	62	143.7	−40.1
R1-2	CO + H → CHO	113.6	92.1	102.8	66.5
R1-3	CO + H → COH	165.9	84.8	151	61.3
R2-1	C + H → CH	72.3	−34.8	73	23.3
R2-2	CHO + H → CHOH	125	41.1	165	105.2
R2-3	CHO → CH + O	51.2	−80.3	97.1	−56.3
R2-4	CHOH → CH + OH	60.4	−103.9	42.9	−117
R2-5	CHO + H → CH + OH	–	–		
R2-6	CHOH + H → CH + H_2O	71.5	−54.9	55.3	−83.3
R3-1	CH + H → CH_2	48.5	17	107.2	61.5
R3-2	CHO + H → CH_2O	33.1	4.8	56.9	25.6
R3-3	CH_2O + H → CH_2OH	79	18.1	142.5	76.4
R3-4	CHOH + H → CH_2OH	49	−18.2	57	−3.2
R3-5	CH_2O → CH_2 + O	27.2	−27.3	83.8	−46.9
R3-6	CH_2OH → CH_2 + OH	64.6	−82.2	42.2	9112.1
R3-7	CH_2O + H → CH_2 + OH	40.8	−64.1	98.3	−35.7
R3-8	CH_2OH + H → CH_2 + H_2O	87.8	−6	–	–
R3-9	CHO+H → CH_2 + O	–	–	–	–
R3-10	CHOH + H → CH_2 + OH	–	–	72	−115.3
R4-1	CH_2+H→CH_3	45.2	−46.1	53.6	−13.8
R4-2	CH_2O + H → CH_3O	56.1	−36.8	82.6	−16.2
R4-3	CH_3O → CH_3 + O	130.7	−47.2	140.1	−57.8
R4-4	CH_3O+H → CH_3 + OH	–	–	–	–
R4-5	CH_2O + H → CH_3+O	30	−84	–	–
R4-6	CH_2OH + H → CH_3 + OH	62.3	−78.4	46.5	−96.4
R4-7	CH_3O + H → CH_3OH	134.4	38.6	158.4	72.6
R4-8	CH_2OH + H → CH_3OH	64.5	−16.3	60.2	−20

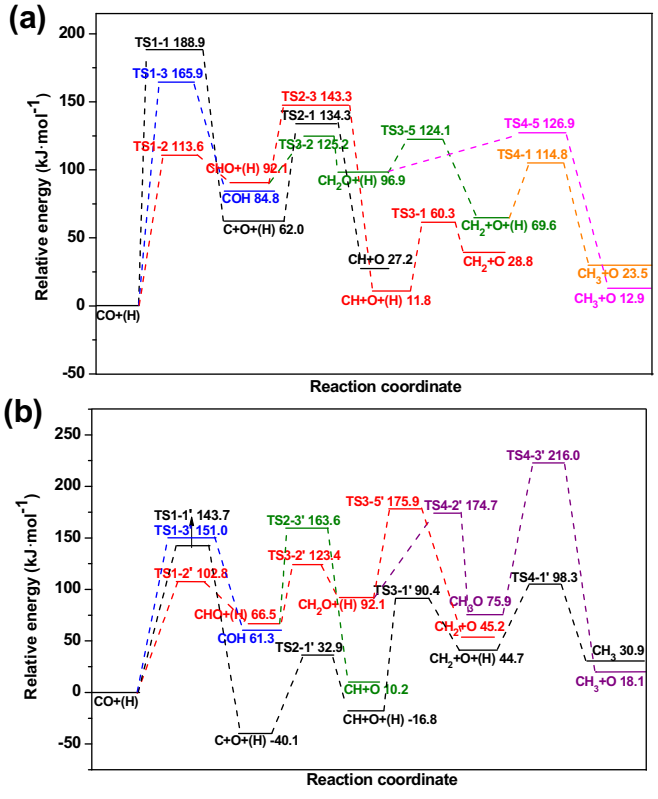

Fig. 3. The potential energy profiles of CH_x hydrogenation pathway and the optimal H-assisted CO dissociation pathway for CH_x(x = 1–3) formation with respect to CO + H species on Co(10$\bar{1}$0)-A and (b) Co(10$\bar{1}$1) surfaces.

CO + H → C + O + H → CH + O (R1-1′, R2-1′), becomes more favorable for CH formation than the optimal H-assisted CO dissociation pathway of CO + H → CHO → CH + O (R1-2′, R2-3′) both dynamically (143.7 vs. 163.6 kJ mol^{-1}) and thermodynamically (−16.8 vs. 10.2 kJ mol^{-1}); meanwhile, CO direct dissociation is also favorable than CO hydrogenation to COH (151.0 and 61.3 kJ mol^{-1}). Thus, CO direct dissociation pathway, CO + H → C + O + H → CH + O, dominantly contributes to CH formation on Co(10$\bar{1}$1) surface.

3.2.2. CH_2 formation

Starting from CH + H, CHO + H, CHOH + H, CH_2O, CH_2OH, CH_2O + H and CH_2OH + H, nine pathways with ten reactions (R3-1–R3-10) may lead to CH_2 formation, as listed in Table 1. R3-1 is the reaction of CH hydrogenation to CH_2, R3-2–R3-10 are the reactions related to CH_2 formation via CHO intermediate (H-assisted CO dissociation pathway).

As shown in Fig. 3(a), on Co(10$\bar{1}$0)-A surface, with respect to CO + H species, the optimal pathway of CO + H → CHO → CH + O + H → CH_2 + O (R1-2, R2-3, R3-1) has the overall barrier and reaction energy of 143.3 and 28.8 kJ mol^{-1}, respectively. However, the optimal H-assisted CO dissociation pathway of CO + H → CHO + H → CH_2O → CH_2 + O (R1-2, R3-2, R3-5) has the overall barrier and reaction energy of 125.2 and 69.6 kJ mol^{-1}, respectively, which is also much favorable than CO direct dissociation (188.9 kJ mol^{-1}) and CO hydrogenation to COH (165.9 kJ mol^{-1}) in kinetics, as a result, the optimal H-assisted CO dissociation pathway of CO + H → CHO + H → CH_2O → CH_2 + O dominantly contributes to CH_2 formation.

As shown in Fig. 3(b), on Co(10$\bar{1}$1) surface, the optimal H-assisted CO dissociation pathway of CO + H → CHO + H → CH_2O → CH_2 + O (R1-2′, R3-2′, R3-5′) has the overall barrier and reaction energy of 175.9 and 45.2 kJ mol^{-1}, respectively. However, CO direct dissociation pathway of CO + H → C + O + H → CH + O + H → CH_2 + O (R1-1′, R2-1′, R3-1′) has the overall barrier and reaction energy of 143.7 and 44.7 kJ mol^{-1}, respectively, which is also favorable than CO hydrogenation to COH (151.0 and 61.3 kJ mol^{-1}). Therefore, CO direct dissociation pathway is dominantly responsible for CH_2 formation on Co(10$\bar{1}$1) surface.

3.2.3. CH_3 formation

Starting from CH_2+H, CH_2O+H, CH_3O and CH_3O+H, as shown in Table 1, six pathways with six reactions for CH_3 formation (R4-1–R4-6) have been considered. R4-1 is the reaction of CH_2 hydrogenation to CH_3, R4-2–R4-6 are the reactions related to CH_3 formation via the H-assisted CO dissociation pathway.

As shown in Fig. 3(a), on Co(10$\bar{1}$0)-A surface, with respect to CO + H species, the optimal pathway of $CO+H\rightarrow CHO+H\rightarrow CH_2O\rightarrow CH_2+O+H\rightarrow CH_3+O$ (R1-2, R3-2, R3-5, R4-1) has the overall barrier and reaction energy of 125.2 and 23.5 kJ mol^{-1}, respectively, meanwhile, the optimal H-assisted CO dissociation pathways of $CO+H\rightarrow CHO+H\rightarrow CH_2O+H\rightarrow CH_3+O$ (R1-2, R3-2, R4-5) has the overall barrier and reaction energy of 126.9 and 12.9 kJ mol^{-1}, respectively. As a result, above two pathways dominantly contribute to CH_3 formations.

As shown in Fig. 3(b), on Co(10$\bar{1}$1) surfaces, the optimal H-assisted CO dissociation pathway of $CO+H\rightarrow CHO+H\rightarrow CH_2O+H\rightarrow CH_3O\rightarrow CH_3+O$ (R1-2′, R3-2′, R4-2′, R4-3′) has the overall barrier and reaction energy of 216.0 and 18.1 kJ mol^{-1}, respectively. However, the CO direct dissociation pathway of $CO+H\rightarrow C+O+H\rightarrow CH+O+H\rightarrow CH_2+O+H\rightarrow CH_3+O$ (R1-1′, R2-1′, R3-1′, R4-1′) has the overall barrier and reaction energy of 143.7 and 30.9 kJ mol^{-1}, respectively, which is also favorable than CO hydrogenation to COH (151.0 and 61.3 kJ mol^{-1}). Thus, CO direct dissociation pathway of $CO+H\rightarrow C+O+H\rightarrow CH+O+H\rightarrow CH_2+O+H\rightarrow CH_3+O$ is dominantly responsible for CH_3 formation.

3.3. General discussion

3.3.1. The effect of surface structure on the formation pathways and existence form of CH_x

Fig. 4 presents the most favorable pathways of CH_x formation on Co(10$\bar{1}$0)-A surface. It can be seen that, H-assisted CO dissociation pathway of $CO+H\rightarrow CHO\rightarrow CH+O$ dominantly contributes to CH formation. H-assisted CO dissociation pathway of $CO+H\rightarrow CHO+H\rightarrow CH_2O\rightarrow CH_2+O$ is mainly responsible for CH_2 formation. For CH_3 formation, there are two parallel H-assisted CO dissociation pathways of $CO+H\rightarrow CHO+H\rightarrow CH_2O\rightarrow CH_2+O+H\rightarrow CH_3+O$ and $CO+H\rightarrow CHO+H\rightarrow CH_2O+H\rightarrow CH_3+O$. Thus, CH_x formation dominantly goes through H-assisted CO dissociation pathways on Co(10$\bar{1}$0)-A surface.

Fig. 5 presents the most favorable pathways of CH_x formation on Co(10$\bar{1}$1) surface, suggesting that CH_x formation mainly proceeds through CO direct dissociation into O and C atoms, followed by C successive hydrogenation to CH_x species, namely, CH_x formation will be dominantly carried out by CO direct dissociation pathways of $CO+xH\rightarrow C+O+xH\rightarrow CH_x$ on Co(10$\bar{1}$1) surface.

Previous studies by Liu et al. [17] have systematically investigated CO activation on different fcc and hcp Co surfaces, their results show that direct CO dissociation is preferred over hcp surfaces while H-assisted dissociation is found over fcc. In fact, CO direct dissociation mainly focus on the hcp Co(11$\bar{2}$1), Co(10$\bar{1}$1), Co(10$\bar{1}$2) and Co(11$\bar{2}$0) surfaces, whereas CO direct dissociation on Co(10$\bar{1}$0)-A surface has a higher activation barrier of 172.7 kJ mol^{-1} with the lower reaction rate of 2.0×10^{7} s^{-1} site^{-1}, moreover, the fcc Co(100), (311) and (110) surfaces is more favorable CO direct dissociation than the hcp Co(10$\bar{1}$0)-A surface. Since CO mainly focuses H-assisted dissociation on fcc Co surfaces, CO activation on Co(10$\bar{1}$0)-A surface should also prefer to be the H-assisted dissociation, our present results confirm that CO activation on Co(10$\bar{1}$0)-A prefers the H-assisted dissociation. On the other hand, the studies by Liu et al. [17] also shown that CO direct dissociation on Co(10$\bar{1}$1) surface has an activation barrier of 116.7 kJ mol^{-1} with the reaction rate of 2.7×10^{14} s^{-1} site^{-1}, meanwhile, compared to the direct route from $CO+H\rightarrow C+O+H$, the H-assisted route from $CO+H\rightarrow CHO\rightarrow CH+O$ are kinetically unfavorable, which agree with our results that CO activation prefers to the H-assisted dissociation on Co(10$\bar{1}$1) surface.

From Fig. 4, we can see that the formation pathways of CH_2 and CH_3 species have the overall barriers of 125.2 and 125.2 (126.9) kJ mol^{-1}, respectively, which are lower than those for CH and C formations, as a result, CH_2 and CH_3 are the most abundant CH_x species to join in chain growth in F-T synthesis on Co(10$\bar{1}$0)-A surface.

As presented in Fig. 5, on Co(10$\bar{1}$1) surface, C coupling has an activation barrier of 192.1 kJ mol^{-1}, which is higher than that of C hydrogenation to CH with an activation barrier of 73.0 kJ mol^{-1}, and CH dissociation has an activation barrier of 49.7 kJ mol^{-1}. CH hydrogenation to CH_2 has an activation barrier of 107.2 kJ mol^{-1}, and that of its back reaction is 45.7 kJ mol^{-1}. CH_2 hydrogenation to CH_3 has an activation barrier of 53.6 kJ mol^{-1}, and that of its back reaction is 67.4 kJ mol^{-1}. In addition, CH_3 hydrogenation to CH_4 has an activation barrier of 92.3 kJ mol^{-1} and its back activation barrier is 109.0 kJ mol^{-1}. These results show that surface C can be easily hydrogenated to CH rather than its coupling, both CH and CH_2 hydrogenation are more difficult than CH_2 dissociation. Thus, among all CH_x species, C and CH species are expected to be the most abundant species. About C species, it is worth mentioning that previous studies about the effect of C covering Co surface on CO activation have indicated that C on the corrugated Co(11$\bar{2}$1) surface will decrease its activity [43], meanwhile, in this study, the high adsorption energy of C means the tight binding and the low CO dissociation barrier on the corrugated Co(10$\bar{1}$1) surface, which can accord with the results reported by Liu et al. [17], suggesting that the activity of the corrugated Co(10$\bar{1}$1) surface may be reduced by C covering, thus, the lower CO dissociation barrier and the higher stability of C should be balanced.

Above results show that the differences of CH_x preferential formation pathway between Co(10$\bar{1}$0)-A and Co(10$\bar{1}$1) surfaces can be attributed to that Co(10$\bar{1}$0)-A surface exhibits the low catalytic activity towards CO direct dissociation, and reduces the possibility of C hydrogenation to CH_x. However, on Co(10$\bar{1}$1) surface, the pathway of CO direct dissociation into C, followed by C successive hydrogenation to CH_x species is more favorable than that CO hydrogenation to CH_xO, followed by its C—O bond scission to CH_x species; suggesting that the hexahedron Co surface structure can affect the preferential formation pathways of CH_x species.

On the other hand, the dominant existence of CH_x species on Co(10$\bar{1}$0)-A and Co(10$\bar{1}$1) are different, both CH_2 and CH_3 are the most abundant CH_x species on Co(10$\bar{1}$0)-A surface, both C and CH species are the most abundant species Co(10$\bar{1}$1) surfaces, indicating that the hexahedron Co surface structure can also affect the dominant existence form of CH_x species. It should be noted that when CH_3 species on Co(10$\bar{1}$0)-A surface is involved in chain growth, the role of CH_3 in FT chain growth must surely be limited, it can only act as an end for alkanes.

3.3.2. The effect of methanol formation on CH_x formation

Since methanol may be formed from syngas in FTS process over Co-based/doped catalysts [44–46], in order to probe into the effect of CH_3OH formation on CH_x formation, we firstly investigate the mechanism of CH_3OH formation. With respect to CO + H species, three pathways may be responsible for CH_3OH formation: $CO+H\rightarrow CHO+H\rightarrow CHOH+H\rightarrow CH_2OH+H\rightarrow CH_3OH$, $CO+H\rightarrow CHO+H\rightarrow CH_2O+H\rightarrow CH_2OH+H\rightarrow CH_3OH$ and $CO+H\rightarrow CHO+H\rightarrow CH_2O+H\rightarrow CH_3O+H\rightarrow CH_3OH$.

Figs. S9 and S10 present the summary potential energy diagram of CH_3OH formation from syngas on Co(10$\bar{1}$0)-A

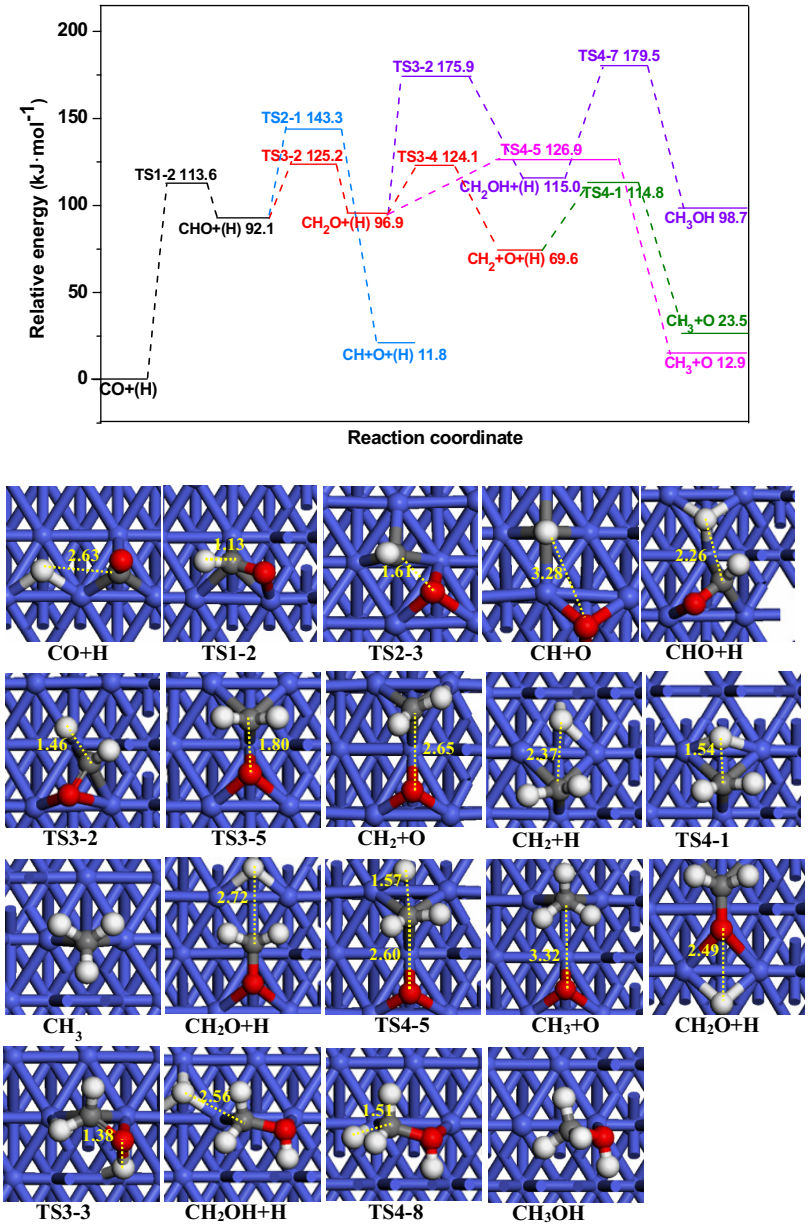

Fig. 4. The potential energy profile for the optimal paths of CHx(x = 1–3) and CH_3OH formation together with the structures of initial states (ISs), transition states (TSs) and final states (FSs) on Co(10$\bar{1}$1) surface. See Fig. 2 for color coding. Bond lengths are in Å.

and Co(10$\bar{1}$1) surfaces, respectively. The calculated results show that above three pathways on Co(10$\bar{1}$0)-A surface have the corresponding overall barriers of 217.1, 179.5 and 194.5 kJ mol^{-1}, respectively. As a result, the pathway of $CO + H \rightarrow CHO + H \rightarrow CH_2O + H \rightarrow CH_2OH + H \rightarrow CH_3OH$ is the dominant pathway of CH_3OH formation on Co(10$\bar{1}$0)-A surface. On Co(10$\bar{1}$1) surface, the overall barriers of these three pathways are 231.5, 234.6 and 234.3 kJ mol^{-1}, respectively, suggesting that these three parallel pathways dominantly contributes to CH_3OH formation. Moreover, previous studies by Cheng et al. [47] have extensively calculated two pathways of CH_3OH formation on both flat and stepped Co(0001), (i) $CO + H \rightarrow CHO + H \rightarrow CH_2O + H \rightarrow CH_3O + H \rightarrow CH_3OH$; (ii) $CO + H \rightarrow COH + H \rightarrow CHOH + H \rightarrow CH_2OH + H \rightarrow CH_3OH$; the results show that the pathway via CHO is thermodynamically and kinetically more favored than the pathway via COH on both the flat and stepped Co(0001), which is in agreement with our present result that CH_3OH is formed via CHO pathway. Meanwhile, the stepped Co(0001) surface are generally more favorable for CH_3OH formation than the flat surface, suggesting that these reactions prefer to occur on the step sites. Above results on different hexahedron Co surfaces suggest that the hexahedron Co surface structure can also affect the preferential formation pathways and the catalytic activity of CH_3OH formation, which agree with our present results.

From Figs. 4 and 5, we can obtain that CHx(x = 1–3) formation is more favorable both dynamically and thermodynamically than CH_3OH formation on the hexahedron Co(10$\bar{1}$0)-A and Co(10$\bar{1}$1) surfaces. Thus, the hexahedron Co(10$\bar{1}$0)-A and Co(10$\bar{1}$1) surfaces exhibit lower catalytic activity for CH_3OH formation, namely, both surfaces can provide more CH_x sources. More importantly, considering both Co(10$\bar{1}$0)-A and Co(10$\bar{1}$1) surfaces cover 63% of the total surface area exposed under the certain realistic conditions, which depend on the conditions, particle size, catalyst support, carbon deposition and many other factors, the contribution to the overall CH_x sources from Co(10$\bar{1}$0)-A and Co(10$\bar{1}$1) surfaces even surpasses that of other hexahedron Co surfaces. Therefore, the hexahedron

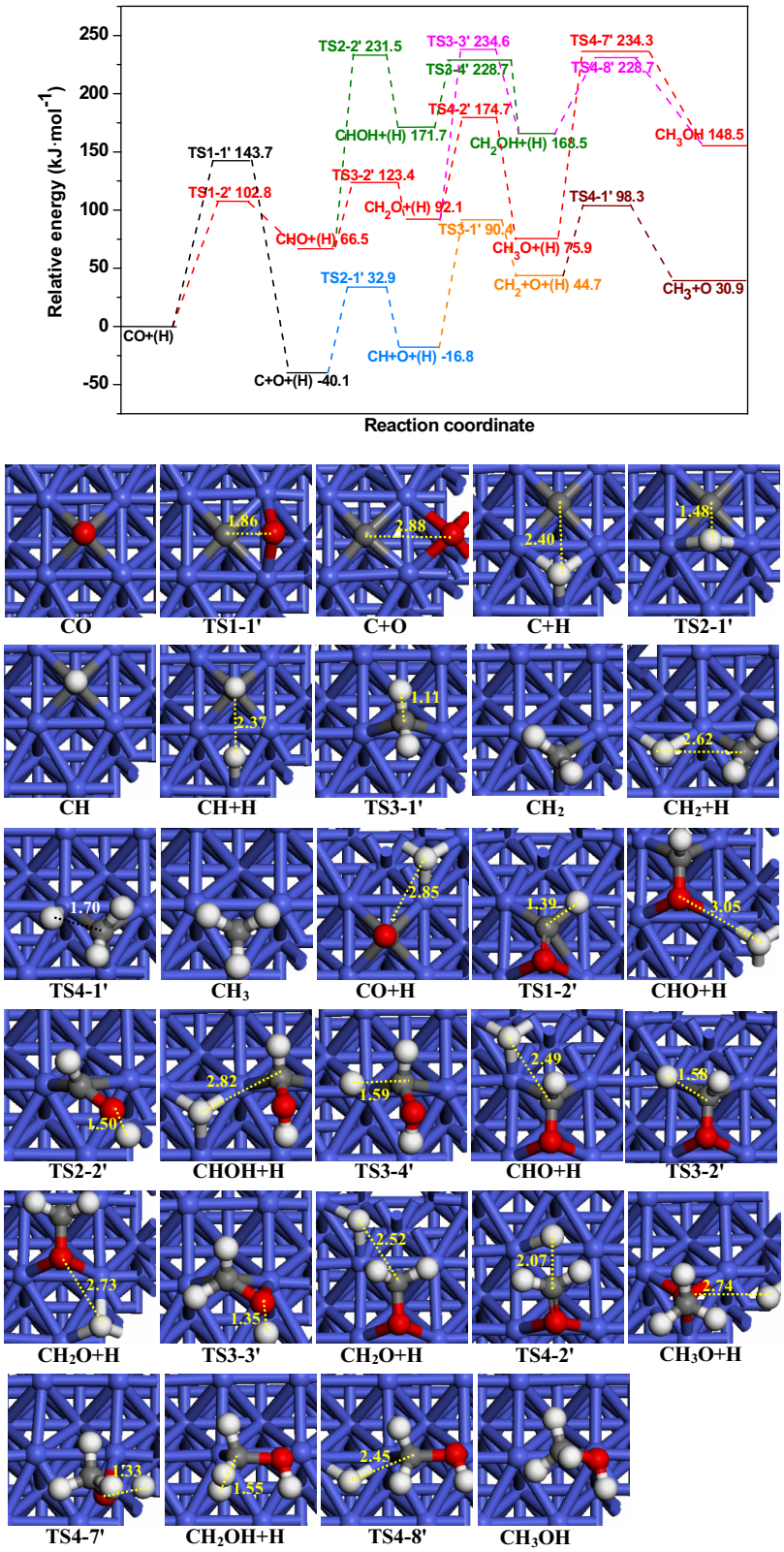

Fig. 5. The potential energy profile for the optimal paths of CHx(x = 1–3) and CH_3OH formation together with the structures of initial states (ISs), transition states (TSs) and final states (FSs) on Co(10$\bar{1}$1) surface. See Fig. 2 for color coding. Bond lengths are in Å.

Co surfaces exhibit high catalytic selectivity for CH_x formation, and provide more CH_x sources to participate into the FTS. Further, the investigations about the effect of the hexahedron Co surfaces will provide the valuable information for developing more efficient and stable Co catalysts with higher mass-specific reactivity for CH_x formation from syngas in FTS. In addition, starting from CH_x species, reducing methane selectivity is one of the main challenges with

Co-catalyzed FTS, which have not been considered in this study, our present studies only focus on CH_x formation.

4. Conclusion

We have used density functional theory calculations to investigate the formation of CH_x species from syngas on the hexahedron Co(10$\bar{1}$0)-A and Co(10$\bar{1}$1) surfaces, which have the corresponding higher surface energy about 35% and 28% of the total surface area exposed, respectively. Our results show that CH_x formation dominantly proceeds through H-assisted CO dissociation pathway on Co(10$\bar{1}$0)-A surface, both CH_2 and CH_3 are the abundant surface CH_x species rather than C and CH. However, CH_x formation goes through CO direct dissociation pathway on Co(10$\bar{1}$1) surface, both C and CH are the abundant surface CH_x species. Co surface structure can affect the preferential formation pathway and the dominant existence form of CH_x species. Moreover, Co(10$\bar{1}$0)-A and Co(10$\bar{1}$1) surfaces present the good catalytic performance for CH_x formation rather than CH_3OH formation, thus, considering both Co(10$\bar{1}$0)-A and Co(10$\bar{1}$1) surfaces cover 63% of the total surface area exposed, the hexahedron Co surface can provide more CH_x sources to participate into FTS. In addition, the present studies only focus on exploring CH_x formation in the chain growth of FTS, on the basis of the dominant existence form of CH_x species, the chain growth of FTS is going on.

Acknowledgments

This work is financially supported by the National Natural Science Foundation of China (Nos. 21276003, 21476155 and 21276171), the Natural Science Foundation of Shanxi Province (No. 2014011012-2), the Program for the Top Young Academic Leaders of Higher Learning Institutions of Shanxi, and the Top Young Innovative Talents of Shanxi.

Appendix A. Supplementary data

Supplementary data associated with this article can be found, in the online version, at http://dx.doi.org/10.1016/j.apcata.2016.07.007.

References

[1] M.E. Dry, Appl. Catal. A: Gen. 138 (1996) 319–344.
[2] A.Y. Khodakov, W. Chu, P. Fongarland, Chem. Rev. 107 (2007) 1692–1744.
[3] M.E. Dry, Catal. Today 71 (2002) 227–241.
[4] B.H. Davis, Ind. Eng. Chem. Res. 46 (2007) 8938–8945.
[5] M.C. Valero, P. Raybaud, Catal. Lett. 143 (2013) 1–17.
[6] A.Y. Khodakov, Catal. Today 144 (2009) 251–257.
[7] H. Schulz, Appl. Catal. A: Gen. 186 (1999) 3–12.
[8] F. Fischer, H. Tropsch, Brennst. Chem. 7 (1926) 97–104.
[9] H. Pichler, H. Schulz, Chem. Ing. Tech. 42 (1970) 1162–1174.
[10] M.P. Andersson, F. Abild-Pedersen, I.N. Remediakis, T. Bligaard, G. Jones, J. Engbæk, O. Lytken, S. Horch, J.H. Nielsen, J. Sehested, J.R. Rostrup-Nielsen, J.K. Nørskov, I. Chorkendorff, J. Catal. 255 (2008) 6–19.
[11] T. Zubkov, G.A. Morgan, J.T. Yates, Chem. Phy. Lett. 362 (2002) 181–184.
[12] U. Bardi, G. Rovida, Stud. Surf. Sci. Catal. 48 (1989) 49–57.
[13] X.Q. Gong, R. Raval, P. Hu, Surf. Sci. 562 (2004) 247–256.
[14] S. Sharan, A.P.J. Jansen, R.A.V. Santen, J. Am. Chem. Soc. 131 (2009) 12874–12875.
[15] Q.F. Ge, M. Neurock, J. Phy. Chem. B 110 (2006) 15368–15380.
[16] J.X. Liu, H.Y. Su, W.X. Li, Catal. Today 215 (2013) 36–42.
[17] J.X. Liu, H.Y. Su, D.P. Sun, B.Y. Zhang, W.X. Li, J. Am. Chem. Soc. 135 (2013) 16284–16287.
[18] S. Shetty, R.A.V. Santen, Catal. Today 171 (2011) 168–173.
[19] H. Papp, Surf. Sci. 129 (1983) 205–218.
[20] O.R. Inderwildi, S.J. Jenkins, J. Phys. Chem. C 112 (2008) 1305–1307.
[21] R. Ojeda, A.U. Nabar, A. Nilekar, M. Ishikawa, J. Catal. 272 (2010) 287–297.
[22] K.F. Zhuo, A. Tan, J. Phys. Chem. C 113 (2009) 8357–8365.
[23] C.F. Huo, Y.W. Li, J.G. Wang, H.J. Jiao, J. Phys. Chem. C 112 (2008) 14108–14116.
[24] P. van Helden, J.A.V.D. Berg, I.M. Ciobîcă, Catal. Sci. Technol. 2 (2012) 491–494.
[25] C.B. Chen, Q. Wang, G.R. Wang, B. Hou, L.T. Jia, D.B. Li, J. Phys. Chem. C 120 (2016) 9132–9147.
[26] E. van Steen, M. Claeys, M.E. Dry, J. van de Loosdrecht, E.L. Viljoen, J.L. Visagie, J. Phys. Chem. B 109 (2005) 3575–3577.
[27] P. van Helden, J.A. van den Berg, C.J. Weststrate, ACS Catal. 2 (2012) 1097–1107.
[28] X.Q. Zhao, S. Veintemillas-Verdaguer, O. Bomati-Miguel, M.P. Morales, H.B. Xu, Phys. Rev. B: Condens. Matter 71 (2005) 024106–024112.
[29] X.B. Hao, Q. Wang, D.B. Li, R.G. Zhang, B.J. Wang, RSC Adv. 4 (2014) 43004–43011.
[30] R.G. Zhang, G.R. Wang, B.J. Wang, J. Catal. 305 (2013) 238–255.
[31] W.X. Pan, R. Cao, G.L. Griffin, J. Catal. 114 (1988) 447–456.
[32] R.L. Toomes, D.A. King, Surf. Sci. 349 (1996) 1–18.
[33] M. Lindroos, C.J. Barnes, P. Hu, D.A. King, Chem. Phys. Lett. 173 (1990) 92–96.
[34] H. Over, G. Kleinle, G. Ertl, W. Moritz, K.H. Ernst, H. Wohlgemuth, K. Christmann, E. Schwarz, Surf. Sci. 254 (1991) L469–L474.
[35] G. Kresse, J. Furthmüller, Comput. Mater. Sci. 6 (1996) 15–50.
[36] G. Kresse, J. Furthmüller, Phys. Rev. B: Condens. Matter 54 (1996) 11169–21118.
[37] J.P. Perdew, J.A. Chevary, S.H. Vosko, K.A. Jackson, M.R. Pederson, D.J. Singh, C. Fiolhais, Phys. Rev. B: Condens. Matter 46 (1992) 6671–6687.
[38] H.J. Monkhorst, J.D. Pack, Phys. Rev. B: Condens. Matter 13 (1976) 5188–5192.
[39] D. Sheppard, P. Xiao, W. Chemelewski, D.D. Johnson, G. Henkelman, J. Chem. Phys. 136 (2012) 074103-1–074103-8.
[40] S. Daniel, T. Rye, H. Graeme, J. Chem. Phys. 128 (2008), 134106-1-10.
[41] G. Henkelman, H. Jónsson, J. Chem. Phys. 111 (1999) 7010–7022.
[42] R.A. Olsen, G.J. Kroes, G. Henkelman, A. Arnaldsson, H. Jónsson, J. Chem. Phys. 121 (2004) 9776–9792.
[43] L. Joos, S. Filot, M. Hensen, V. Van Speybroeck, R.A. van Santen, J. Phys. Chem. C 118 (2014) 5317–5327.
[44] Ø. Åse Marit Leere, E. Uggerud, Chem. Phys. 262 (2000) 169–177.
[45] F. Studt, F. Abild-Pedersen, Q.X. Wu, A.D. Jensen, B. Temel, J.D. Grunwaldt, J.K. Nørskov, J. Catal. 293 (2012) 51–60.
[46] J. Nerlov, S. Sckerl, J. Wambach, I. Chorkendorff, Appl. Catal. A: Gen. 191 (2000) 97–109.
[47] J. Cheng, P. Hu, P. Ellis, S. French, G. Kelly, C. Martin Lok, J. Phys. Chem. C 112 (2008) 9464–9473.